Nanoscale
Advances

rsc.li/nanoscale-advances

ROYAL SOCIETY
OF CHEMISTRY

PAPER
Nikos Tagmatarchis *et al.*
Preclinical evaluation of modified carbon nanohorns and
their complexation with insulin

NCNST

PAPER

Check for updates

Preclinical evaluation of modified carbon nanohorns and their complexation with insulin†

Christina Stangel, [ID] ‡[a] Antonia Kagkoura, [ID] ‡[a] Natassa Pippa, [ID] [b] Dimitris Stellas, [ID] [c] Minfang Zhang, [ID] [d] Toshiya Okazaki, [ID] [d] Costas Demetzos[b] and Nikos Tagmatarchis [ID] *[a]

The current study emphasizes the minimal toxicity observed *in vitro* and *in vivo* for carbon nanohorns (CNHs) modified with third generation polyamidoamine (PAMAM) dendrimers. Initially, we investigated the interactions between CNH–PAMAM and lipid bilayers, which were utilized as representative models of cellular membranes for the evaluation of their toxicity *in vitro*. We found that the majority of those interactions occur between the modified CNHs and the polar groups of phospholipids, meaning that CNH–PAMAM does not incorporate into the lipid chains, and thus, disruption of the lipid bilayer structure is avoided. This outcome is a very important observation for further evaluation of CNH–PAPAM in cell lines and in animal models. Next, we demonstrated the potential of CNH–PAMAM for complexation with insulin, as a proof of concept for its employment as a delivery platform. Importantly, our study provides comprehensive evidence of low toxicity for CNH–PAMAM both *in vitro* and *in vivo*. The assessment of cellular toxicity revealed that the modified CNHs exhibited minimal toxicity, with concentrations of 151 µg mL^{-1} and 349 µg mL^{-1}, showing negligible harm to EO771 cells and mouse embryonic fibroblasts (MEFs), respectively. Moreover, the histological analysis of the mouse livers demonstrated no evidence of tissue necrosis and inflammation, or any visible signs of severe toxicity. These findings collectively indicate the safe profile of CNH–PAMAM and further contribute to the growing body of knowledge on the safe and efficient utilization of CNH-based nanomaterials in drug and protein delivery applications.

Introduction

In recent years, nanotechnology has revolutionized the field of biomedicine, offering unprecedented opportunities for the development of advanced drug delivery systems such as porous organic polymers or stable aqueous nanocolloids for increasing the therapeutic index of various active pharmaceutical ingredients.[1,2] The assembly approach for establishing delivery systems is of paramount importance for the design and development of nanoparticles for targeting specific tissues and organelles.[3,4] Among the plethora of nanomaterials, carbon nanohorns (CNHs) have emerged as a promising class of carbonaceous materials with unique properties that make them well-suited for biomedical applications.[5–8] CNHs, characterized by their cone-shaped tip structure, possess a range of advantageous features, including high purity, low toxicity, biodegradability, and excellent biocompatibility. These inherent properties, coupled with their versatile surface chemistry, render CNHs an attractive platform for various biomedical applications, particularly as innovative drug carriers.[6–10]

CNHs have shown great potential as drug delivery systems due to their unique morphology and biocompatibility. They have been shown to effectively encapsulate drugs and biomolecules, protecting them from degradation and improving their bioavailability.[11,12] Moreover, their small size and high surface area allow them to penetrate cellular membranes and deliver drugs directly to targeted cells, making them an attractive option for targeted drug delivery. In addition, the biodistribution and hydrophilicity of CNHs is notably affected by the type of chemical functionalization they undergo.[8,13] Moreover, oxidation of CNHs results in the creation of nanoscale apertures along the sidewalls, enabling the infiltration of a wide range of small biomolecules into the inner cavity, facilitating the controlled and gradual release of biomolecules.[14,15] Furthermore, openings at the tips of CNHs permit the

[a]*Theoretical and Physical Chemistry Institute, National Hellenic Research Foundation, 48 Vassileos Constantinou Avenue, Athens 11635, Greece. E-mail: tagmatar@eie.gr*

[b]*Section of Pharmaceutical Technology, Department of Pharmacy, School of Health Sciences, National and Kapodistrian University of Athens, Athens 15771, Greece*

[c]*Institute of Chemical Biology, National Hellenic Research Foundation, 48 Vassileos Constantinou Avenue, Athens 11635, Greece*

[d]*Nano Carbon Device Research Center, National Institute of Advanced Industrial Science and Technology (AIST), Tsukuba 305-8565, Japan*

† Electronic supplementary information (ESI) available. See DOI: https://doi.org/10.1039/d3na00471f

‡ These authors have equally contributed to this work.

introduction of diverse substances, including pharmaceutical drugs, which can be stored within the nanostructure and subsequently released.[16] Interestingly, covalent functionalization approaches introduce functional groups that can be utilized to further customize CNHs with suitable drugs,[17,18] biomolecules, or liposomes,[19] increasing solubility at the same time. Within this context, cycloaddition reactions were employed to covalently attach polyamidoamine (PAMAM) dendrimers onto the surface of CNHs to serve as effective bio carriers.[20–22]

Markedly, CNHs demonstrate enhanced biocompatibility and safety in comparison to carbon nanotubes (CNTs).[23] However, the toxicity of both CNHs and CNTs is contingent upon the method of functionalization. Notably, the absence of metal impurities in CNHs, unlike other carbon-based nanomaterials, has been identified as a crucial factor in mitigating potential carcinogenic hazards in cellular environments.[24] Although the toxicity of CNHs is well-established in the literature, the mechanism of their incompatibility is still under investigation. Generally, the degree of cellular uptake, the mechanism of internalization, localization into cells, as well as the expression of inflammatory cytokines, are strongly dependent on the colloidal dispersion, the shape, and the surface modification and charge of nanohorns.[25,26] Namely, CNH aggregates promote mitochondrial dysfunction-induced apoptosis in hepatoblastoma cells by targeting sirtuin 3, which is a short-chain protein expressed in this subcellular organelle.[27] The presence of CNH aggregates upregulates the expression of sirtuin 3, which leads to the cascade of the apoptosis mechanism. Combinations of CNHs with other materials, such as lipids, polymers and magnetic nanoparticles, have been used to ameliorate their biocompatibility and for drug delivery and targeting purposes.[19,27] They have also been used to modulate tenocyte cellular response and tendon biomechanics, which are very important for the subfailure ligament and tendon injury.[28,29] For achieving this, oxidized CNHs were immobilized on a titanium surface using material-binding peptides/peptidic aptamers to enable targeted delivery.

PAMAM dendrimers are compact macromolecules with defined chemical structures, known for their nanosized, regularly branched and globular nature.[30] They possess unique characteristics such as biocompatibility, high adsorption capacity, convenient modification of end groups and effective antibacterial properties, making them valuable in biomedicine.[31] Due to precise chemical synthesis, dendrimers exhibit monodispersity, ensuring a uniform shape and size.[32] They can be easily modified by incorporating functional groups and enhancing solubility and reactivity, expanding their practical applications. This modification capability enables precise delivery of drugs, genetic material, antibodies, and signaling molecules into cells.[33,34] Still, PAMAM dendrimer toxicity hinges on factors like size, surface modifications and concentration. Some studies raise concerns, but well-designed PAMAM dendrimers can safely serve drug delivery and various applications.[34,35] Lower generation PAMAM dendrimers (below G4) with open structures have a higher drug entrapment capacity compared to higher generations (>G6), characterized by a more rigid surface due to increased branching and surface group density.[34] Combining PAMAM dendrimers with carbon nanostructures enhances solubility and modifies structural characteristics, leveraging their unique properties.[36–38] However, the exploration of CNH–PAMAM conjugates is relatively limited in comparison to their counterparts based on CNTs.

In this study, we employed third generation polyamidoamine dendrimers to covalently decorate CNHs and conducted a comprehensive investigation into their toxicity both *in vitro* and *in vivo*. Initially, our focus was on understanding the interaction between CNH–PAMAM and lipid bilayers, which serve as models of cellular membranes, using differential scanning calorimetry (DSC). According to the DSC results, the majority of interactions occurred between the modified CNHs and the polar groups of phospholipids, rather than being incorporated into the lipid chains themselves. To the best of our knowledge, this is one of the first reports where the interactions of modified CNHs carrying polyamidoamine dendrimer units with model lipid bilayers are investigated. Motivated by these findings implying no disruption of the lipid bilayer structure, we studied the behavior of CNH–PAMAM in the dispersion state and explored their potential for complexation with insulin, as a proof of concept for its usage as a delivery platform. The dispersion and the complexes were subjected to physicochemical characterization using dynamic and electrophoretic light scattering techniques. Subsequently, we evaluated the *in vitro* cellular toxicity and carried out *in vivo* studies in mice. Histological analysis of mouse livers revealed no signs of tissue necrosis, inflammation, or any visual indications of severe toxicity. These results underscore the biocompatibility of the modified CNHs and support their potential applicability in various biomedical applications.

Experimental

Methods

Differential scanning calorimetry. The protocol used for the thermodynamic characterization, which utilizes DSC of the lipid bilayers, is described in our previous investigation.[39]

Physicochemical characterization and stability assessment of functionalized CNHs (f-CNHs). For the physicochemical characterization of **f-CNHs** and their stability assessment, we used dynamic and electrophoretic light scattering (DLS and ELS) to evaluate the size/size distribution and ζ-potential of the prepared systems, respectively. Furthermore, the same techniques were used for the characterization of f-CNH:insulin complexes.

Preparation of f-CNH:insulin complexes. The f-CNH:insulin complexes were prepared by adding different amounts of insulin solutions to the f-CNH dispersion of the same volume (300 μL) and concentration (1 mg mL^{-1}), under stirring. Finally, appropriate volumes of HPLC-grade water were added to achieve a constant final volume and ionic strength for all dispersions prepared. Thus, the concentration of **f-CNHs** was kept constant throughout the series of dispersions, while that of insulin varied to control the required ratio of the two components. The dispersions of the complexes were left for

equilibration for an hour. The physicochemical characterization of the complexes was performed by using DLS and ELS, as described in the previous section.

Insulin complexation and complexation efficiency (%EE) studies. The complexation protocol for the loading of all the prepared systems with insulin is described elsewhere.[40] Free insulin was separated from the insulin complexed with **f-CNHs** by using the ultrafiltration centrifugal method. In detail, the complexes were centrifuged for 30 min at 4000 rpm using centrifugal filter tubes [molecular weight (MW) cutoff = 100 kDa; Millipore]. The particles were separated from the aqueous phase, and the free insulin was analyzed in the supernatant by the bicinchoninic acid (BCA) protein quantification method according to the kit protocol. Protein quantification using BCA (Pierce™ BCA Protein Assay Kit, Thermo Scientific ™) protein assay was carried out following the manufacturer's instructions. Briefly, the samples were incubated up to 30 min at 37 °C, with 25 μL of the sample and 200 μL of the working reagent. Absorbance was then measured at 562 nm using an INNO microplate reader. Centrifuged samples of the respective empty carriers were also analysed by BCA assay and used as a blank. The loading % was calculated according to the following equation:

$$(\text{loading})\% = \left(1 - \frac{C_{\text{supernatant}}}{C_{\text{total}}}\right)\%$$

where $C_{\text{supernatant}}$ is the concentration of insulin that was quantified in the supernatant (non-entrapped) and C_{total} is the total concentration of the insulin added in the dispersion.[41]

Cell viability assays. The EO771 cells were purchased from CH3 BioSystems and cultured in a complete RPMI 1640 medium supplemented with 10% fetal calf serum, 100 U mL^{-1} penicillin and 100 mg mL^{-1} streptomycin. Mouse embryonic fibroblasts (MEFs) were generated as a primary cell culture, and subsequently grown in DMEM medium containing 10% fetal bovine serum (FBS), 100 U mL^{-1} penicillin and 100 mg mL^{-1} streptomycin at 37 °C. To test the inhibitory activities of compounds using a cell-based assay, MTT assays were performed for cell viability. Briefly, EO771 cells and MEFs were plated at a density of 3000 cells per well in a 96-well plate. After 24 h, the cells were treated with **f-CNHs** in a dose-dependent manner for 72 h. Viable cell numbers were determined by tetrazolium conversion to its formazan dye. All the experiments were performed three times and the tested concentrations in each experiment were evaluated in quadruplicate wells.

***In vivo* acute toxicity assays.** All animal studies were approved by the National Hellenic Research Foundation (NHRF) Animal Care and Use Committee. The study protocol was approved by the local ethics committee (Athens Prefecture Veterinarian Service; (315856/15-03-2023)). Animal care was provided in accordance with the procedures outlined in the "Guide for Care and Use of Laboratory Animals (National Research Council; 1996; National Academy Press; Washington, D.C.). The *in vivo* study was conducted in the ISO 9001: 2015 operating (registration number I-030-02-100-01430) animal model unit of the Institute of Chemical Biology of the NHRF. Briefly, to study the acute toxicity of the CNHs we injected I.P 6

C57BL/6 female mice, bred in our facility, with **f-CNHs** at a concentration of 100 μg mL^{-1} (the final volume was 200 μL dose^{-1}). Another 6 C57BL/6 female mice were also injected with 200 μL saline and served as our control group. The mice were monitored for any signs of discomfort or morbidity, for a period of 7 days. At the end of the experiment the mice were euthanized and examined macroscopically for signs of acute toxicity, and their livers were collected for subsequent histopathological evaluation.

Histopathological analysis. Mouse livers were surgically removed postmortem, fixed in 10% neutral buffered formalin (NBF, Sigma) and then routinely processed and paraffin embedded. Liver sections were dewaxed and rehydrated and then were stained with hematoxylin and eosin (H&E).

Statistical analysis. Statistical analyses and graph generation were performed with GraphPad Prism 9.2.0 (San Diego, CA, USA).

Results and discussion

Preparation of f-CNHs

The growth of PAMAM dendrimers by *in situ* polymerization onto the CNH surface was accomplished according to Scheme 1, yielding functionalized CNHs (**f-CNHs**). To begin, the aniline derivative *tert*-butyl 2-(2-(2-(4-aminobenzamido)ethoxy)ethoxy) ethylcarbamate **2** was employed to *in situ* generate aryl diazonium salts, resulting in the production of butoxy carbonyl (BOC)-modified CNH-based material **3**. The amino-units were liberated (material **4**), before PAMAM growth was initiated. The process involved the addition of methyl acrylate to the amino groups in material **5** *via* Michael addition, followed by amidation of the terminal ester groups with ethylenediamine, resulting in first-generation PAMAM dendrimers on the surface of CNHs (material **6**). Subsequently, **6** undergoes a two-step reaction with methyl acrylate and ethylenediamine to produce second-generation PAMAM, resulting in material **8**. Performing the same reaction again on **8** leads to an increase in PAMAM generation to third, yielding **f-CNHs**.

The preparation of **f-CNHs** was carefully monitored at each stage using various spectroscopic techniques, including ATR-IR and Raman spectroscopy, as well as thermogravimetric analysis (TGA). Initially, the ATR-IR spectrum of material **3** revealed characteristic bands associated with the carbonyl stretching of the benzamide and BOC protective groups at 1643 and 1701 cm^{-1}, respectively. Additionally, bands ranging at 2833–2980 cm^{-1} were attributed to the C–H bending and stretching modes (Fig. S1†). The ATR-IR spectrum of material **4**, which is based on ammonium-modified CNHs, did not show a band related to the BOC group (Fig. S1†). This provides evidence that the cleavage of the amine units was successful and the BOC group was liberated. The Kaiser test was conducted to confirm the BOC cleavage and it yielded a positive result for the ammonium-modified CNH-based material **4** (93 μmol g^{-1}). The presence of ester carbonyl vibrations can be observed at 1715 cm^{-1} in material **5**, followed by the amide carbonyl vibrations shifted to 1635 cm^{-1} in material **6** (Fig. 1a). A similar pattern is observed for materials **7–9** and **f-CNHs**, where
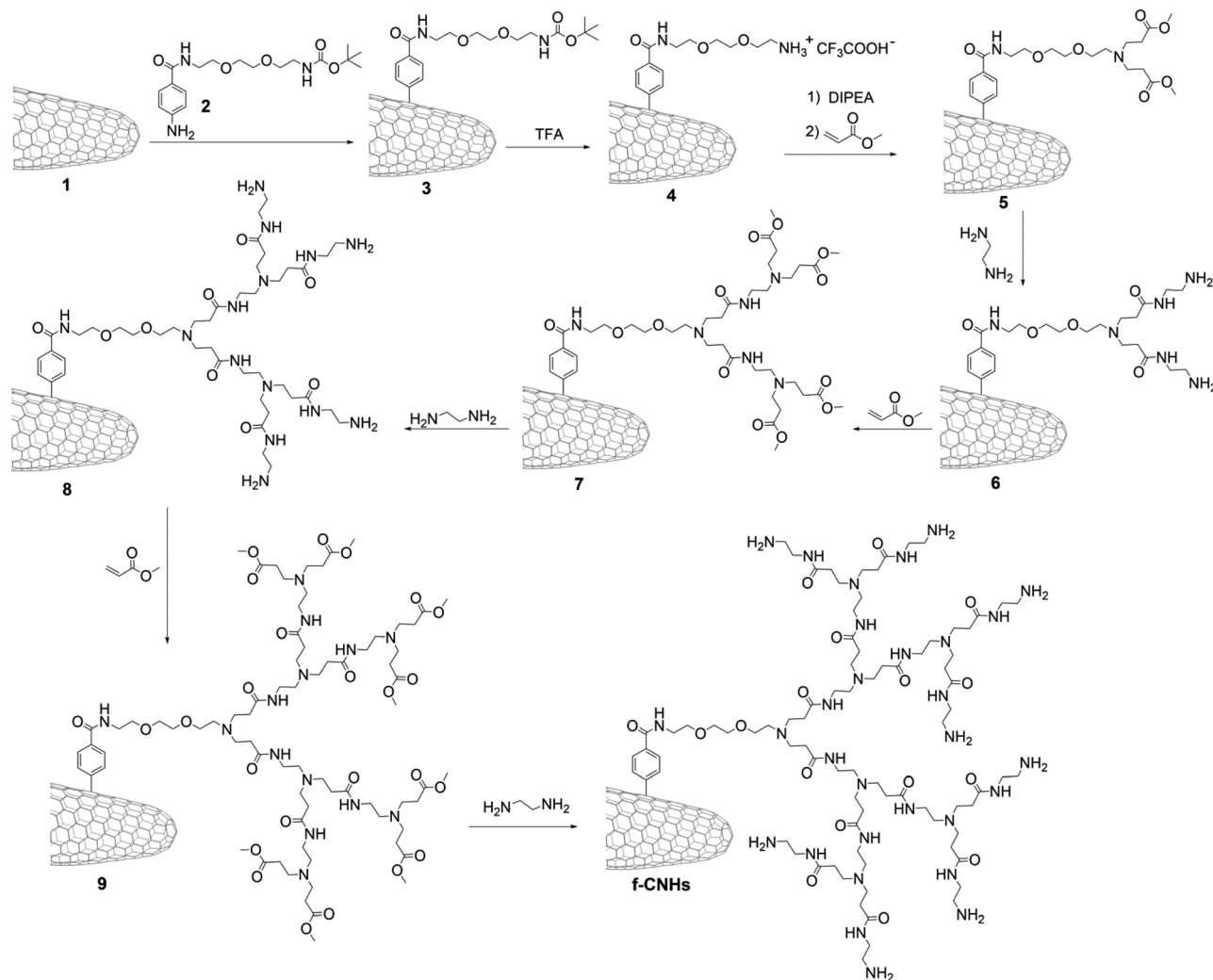
Scheme 1 Illustrative preparation of **f-CNHs**.

vibrations of the ester group are obvious in materials 7 and 9 (Fig. 1a).

The Raman spectra of modified and pristine CNHs were obtained by exciting them at 514 nm. In the Raman spectrum of the latter, there are two bands with similar scattering strengths, namely, the D-band at 1342 cm^{-1} and the G-band at 1587 cm^{-1} (Fig. 1b). The D/G ratio, which is the ratio of the intensities of the two bands, changes from 1.1 for pristine CNHs to 1.3 for 3 and 4. The D-band indicates the density of defects in the CNHs and can be used to monitor the degree of functionalization. Material 3 shows an increase in the intensity of the D-band due to the hybridization changing from sp^2 to sp^3 in the CNH framework caused by the incorporation of the aryl diazonium salt, while the D/G ratio in 4 remains the same as that in 3 because removing the BOC protecting group with acidic treatment does not further disturb the CNH skeleton. The same applies for intermediate steps and the final **f-CNH** material bearing eight amino groups (data are shown in Fig. 1b only for **f-CNHs**). The ATR-IR and Raman spectral results for up to second-generation PAMAM dendrimers align with earlier studies, confirming their consistency with previous findings.[42] The analysis of CNH-based materials continued with thermogravimetric analysis. The TGA data allow us to estimate the loading of organic units attached to the modified CNHs and provide information about the thermal stability of the materials as the temperature changes. Pristine CNHs remain thermally stable under a nitrogen atmosphere up to 800 °C. However, modified-CNHs 3 and 4 begin to decompose at temperatures above 550 °C, after losing their organic addends at 200–550 °C. This occurs due to the gradual destruction of the graphitic skeleton in sp^3 hybridized sites, where functionalization took place. The data presented in Fig. 1c show that materials 3 and 4 experienced a mass loss of 21% and 18%, respectively, in the temperature range of 200–550 °C. The lower mass loss in material 4, compared to material 3, indicates the efficient removal of the BOC protecting group. Based on this, the loading in material 4 was determined to be one functional unit (e.g. one positive charge) for every 94 carbon atoms of CNHs. Furthermore, it is important to note that there is an increase in mass loss during the incremental expansion of PAMAM units (as
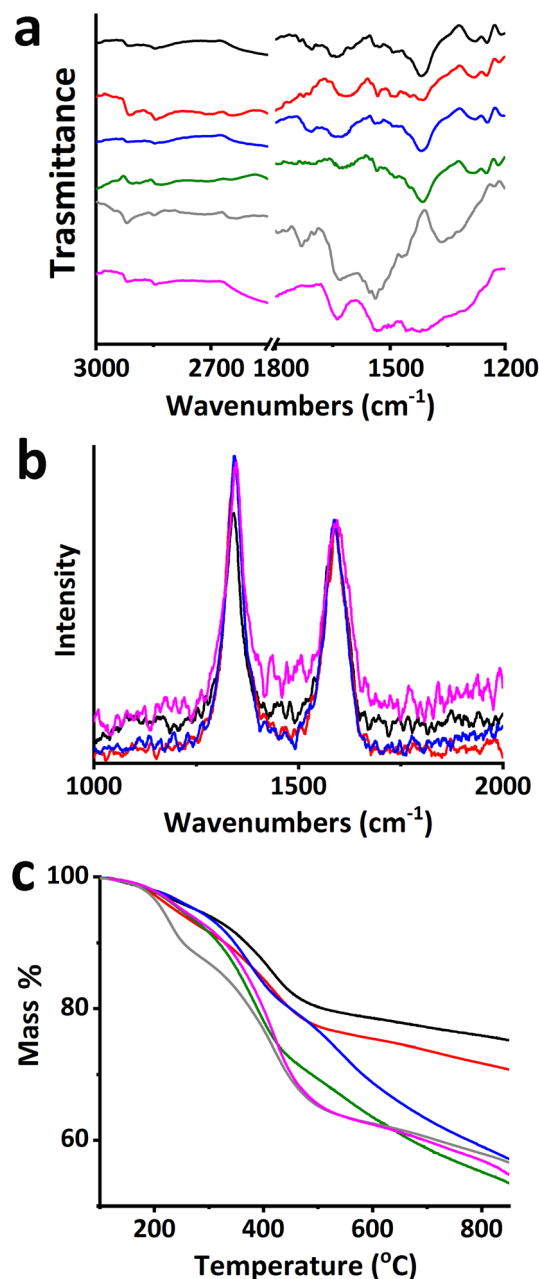
Fig. 1 (a) ATR-IR spectra, (b) Raman spectra (514 nm), and (c) thermogravimetric analysis graphs, obtained under a nitrogen atmosphere, of materials **5** (black), **6** (red), **7** (blue), **8** (green), and **9** (grey) and **f-CNHs** (pink).

depicted in Fig. 1c) from first-generation (23%) to second-generation PAMAM (28%). The mass loss for third-generation PAMAM reaches an unimpressive 31%, while the loading was determined to be one functional unit for every 286 carbon atoms. It should be emphasized that the dendritic units employed in this study are not analogous to the precursors utilized. Probably the strong attachment formed primarily impedes the growth of amido and amino subunits, resulting in a limited yield of PAMAM functionalization.[43] Additionally, the positive Kaiser test with an increased amino-loading of 129, 167

and 201 μmol g^{-1} for **6**, **8** and **f-CNHs**, respectively, verifies the TGA results.

Insight on the morphology of the material was provided by TEM imaging. Briefly, TEM images of high (Fig. 2a and b) and low magnification (Fig. S2†) revealed the presence of amorphous-like species adhering to the surfaces of CNH aggregates and the conical edges. In contrast, pristine CNHs exhibited a purely cone-like structure (Fig. 2c). Moreover, the absence of metal impurities is apparent, in both pristine and modified CNHs, which is an advantage of the material when it is employed in biological assessment. These observations provide additional visual confirmation of the functionalization of CNHs with the PAMAM dendritic units.

Interactions of f-CNHs with models of cellular membranes

DSC is widely used for the study of interactions between different materials.[44] Lipid membranes composed of phospholipids are used as models of cellular membranes. In this investigation, we used DPPC : DPPG (9 : 1 molar ratio) lipid bilayers as a model of a cellular membrane for the quantification of interactions of **f-CNHs** with them. The results from DSC experiments could be a roadmap for the prediction of the toxicity/biocompatibility of **f-CNHs**. The DSC heating and cooling curves of DPPC : DPPG (9 : 1 molar ratio) with increasing concentrations of **f-CNHs** are presented in Fig. 3, while all the calorimetric values are summarized in Table S1.† The calorimetric values of pure DPPC : DPPG (9 : 1 molar ratio) lipid bilayers are in line with the values observed in the literature (Ts, which has a weak peak at around 36 °C, and Tm, which has a sharp peak at around 41 °C, Fig. 3a).[44] As a negative control, we used the pure DPPC : DPPG lipid membranes, and we compared the thermotropic parameters of these pure membranes with those after the addition of the modified CNHs (Table S1† and Fig. 3). It should be pointed out that in the temperature range of the DSC experiments, the **f-CNHs** did not show any thermal event, as expected. For this reason, it can not necessarily be used as a positive control. We observed that the addition of **f-CNHs** caused a decrease in absolute values of ΔHs of the pretransition thermal event. The decrease was higher with an increase in the concentration of **f-CNHs**. The cooperativity of the DPPC : DPPG (9 : 1 molar ratio) lipid bilayers was also differentiated by using the increased concentration of the carbon-nanomaterial guest, as the $\Delta T_{1/2}$ values revealed (Table S1†). These findings revealed interactions of **f-CNHs** with the polar groups of the phospholipids. Namely, the animo groups of **f-CNHs** interacted with the phosphate groups of DPPC and DPPG, causing increased mobility of the polar groups as $\Delta T_{1/2}$ values revealed. These interactions were also concentration-dependent because higher concentration of **f-CNHs** led to a higher increase in $\Delta T_{1/2}$ and ΔHs values (Table S1†). The pretransition temperature (Ts) remained unaffected after the addition of **f-CNHs** (Fig. 3 and Table S1†); however, there was a broadening of the pretransition peak, especially at the highest concentration of **f-CNHs** leading to different lateral organizations (Fig. 3).[40] On the other hand, the addition of **f-CNHs** did not alter the main transition temperature and the transition
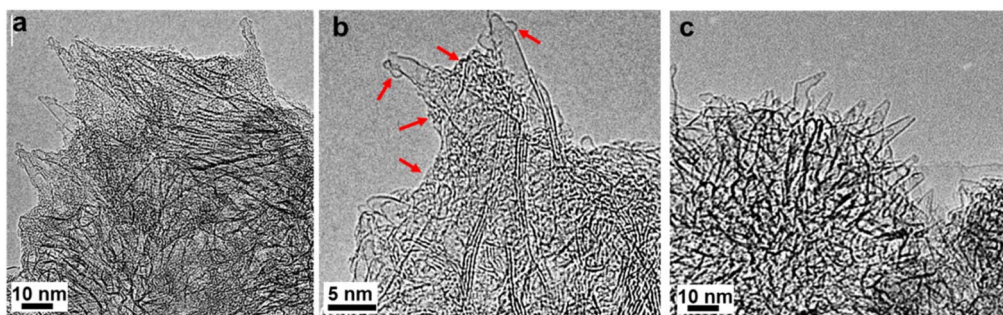
Fig. 2 Representative TEM high magnification images of PAMAM-functionalized **f-CNHs** (a and b) and pristine CNHs (c). The red arrows in (b) highlight the presence of amorphous-like species attached to the surface of CNHs.

enthalpy of the lipid bilayers. There was only a slight increase in Tm and ΔHm at the highest concentration of **f-CNHs**. The strong interaction of **f-CNHs** with polar groups of DPPC/DPPG phospholipids at 1 mg mL^{-1} caused the re-orientation of

phospholipid chains and consequently, a slight differentiation of calorimetric values. The last observation means that there are no interactions between the lipid chains of the lipids with **f-CNHs**. Summarizing all the above from DSC experiments, we
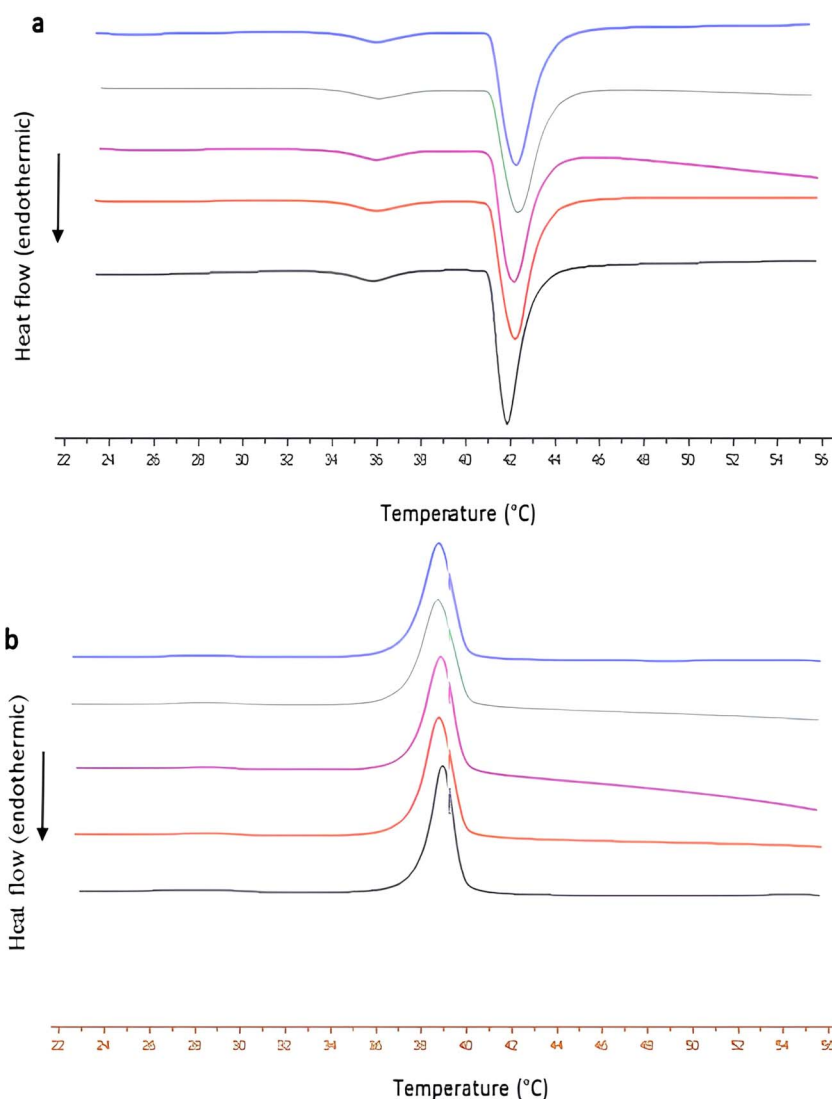

Fig. 3 The DSC (a) heating, and (b) cooling curves of DPPC : DPPG (9 : 1 molar ratio) at 0 (black line), 0.1 (red line), 0.2 (purple line), 0.5 (green line) and 1 mg mL^{-1} (blue line) of **f-CNHs**.

can conclude that **f-CNHs** strongly interact with the polar groups of phospholipids, and there is no incorporation of them into lipid chains, meaning that there is no disruption of the lipid bilayer structure.[43–46] The latter means that the penetration of the carbon-based nanomaterial is limited at concentrations up to 1 mg mL^{-1} (the highest concentration that we used) without any destruction of the structure of the model lipid membranes. Last but not least, the aforementioned results show a quite different behaviour of **f-CNHs** and their interaction with models of lipid membranes, which is the generation of nanoscale holes and the enhancement of membrane permeability.[47]

Physicochemical characterization and stability assessment of f-CNHs

We also studied the colloidal behaviour of **f-CNHs** in HPLC-grade water. The concentration of **f-CNHs** was 1 mg mL^{-1} (appropriate amount of **f-CNHs** was diluted in an appropriate amount of HPLC water followed by 20 min sonication). After the preparation of the **f-CNH** dispersion in an aqueous medium, we measured its physicochemical characteristics (Fig. 4).

The physicochemical characteristics of **f-CNHs** in the dispersion state were evaluated by dynamic and electrophoretic light scattering for their size/size distribution and zeta-potential, respectively. The size of **f-CNHs** was found to be around 1 μm and the size distribution showed a monodisperse population of particles considering the nature of the material and the dilution protocol. The zeta potential values were around 20 mV due to the presence of anino groups on the surface of the carbon-based nanomaterial (Table S2†). The dispersion was stored at 4 °C and we performed stability studies for 40 days. All the physicochemical characteristics remained unaffected for 2

days (Fig. 4). We observed an increase in the size of the colloidal particles at one week and a decrease in scattering intensity values (I-KCps). The population of the particles became polydisperse. After three weeks, the size was around 3 μm and a further decrease in scattering intensity values was observed (Fig. 4 and Table S2†). The same trend was also identified from the measurements forty days after the preparation of the **f-CNH** colloidal system. Aggregation phenomena took place in the dispersion and led to an increase in the Dh and PDI values, accompanied by a decrease in scattering intensity values (Fig. 4 and Table S2†). The presence of van der Waals interactions is responsible for the aggregation phenomena in colloidal dispersions, according to Derjaguin, Landau, Verwey and Overbee's (DLVO) theory for the kinetic stability of nano-colloids. These attractive interactions can overcome the electrostatic repulsions (as zeta potential values revealed). For this reason, coagulates are formed.[48,49] The last observation means that the structure of the coagulates was not compact because the mass of the systems decreased (decrease in scattering intensity values). Additionally, the values of zeta potential showed that the electrostatic repulsion between the coagulates was not strong enough to avoid the aggregation of the **f-CNH** particles.[47] We also should point out that a slight decrease in zeta potential values during the stability studies was observed, meaning that the surface of aggregates/coagulates was quite different from the initially formed dispersed particles, masking their charge network. On the 40th day of the stability studies, sedimentation appeared and for this reason the stability protocol measurements were carried out. The sedimented system was subjected to 20 min sonication to study the potential reversibility of the aggregation process. After the annealing of the system, we also measured all its physicochemical characteristics. The results from the physicochemical characterization showed that there was a decrease in size and the size distribution values, and an increase in the mass of the system (Table S2 and Fig. S3†). The same results were obtained after the sonication of the sedimented systems for 40 min (Table S2 and Fig. S3†). These results revealed that the aggregation phenomena were not reversible with sonication.

Evaluation of f-CNH:insulin complexes

Having in mind the biocompatibility profile and the colloidal behaviour of **f-CNHs**, we decided to load them with a model protein. Insulin was chosen due to its surface charge and low molecular weight in comparison to other proteins. To best of the authors' knowledge, this is the first report in the literature where functionalized nanohorns are used for loading of insulin. Concentration of insulin ranged between 0.001 mg mL^{-1} and 0.05 mg mL^{-1}. The driving force of the complexation process is electrostatic interactions developed between the positive surface charge of **f-CNHs**, as zeta potential values indicated, and negative surface charge of insulin.[50,51] It should be noted that insulin was selected as a model protein due to its physicochemical characteristics, *i.e.*, low molecular weight in comparison to other proteins and negative surface charge. The physicochemical characteristics of the complexes are presented
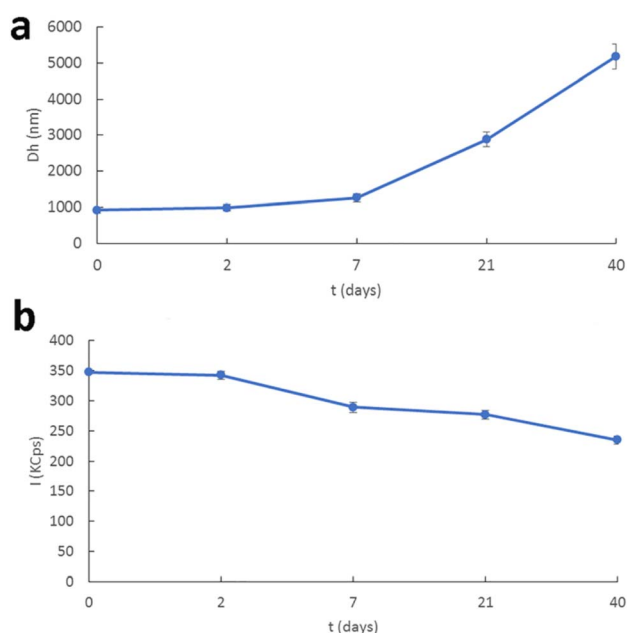

Fig. 4 Stability assessment of **f-CNHs** *via* examination of the (a) hydrodynamic diameter and (b) scattering intensity with time.
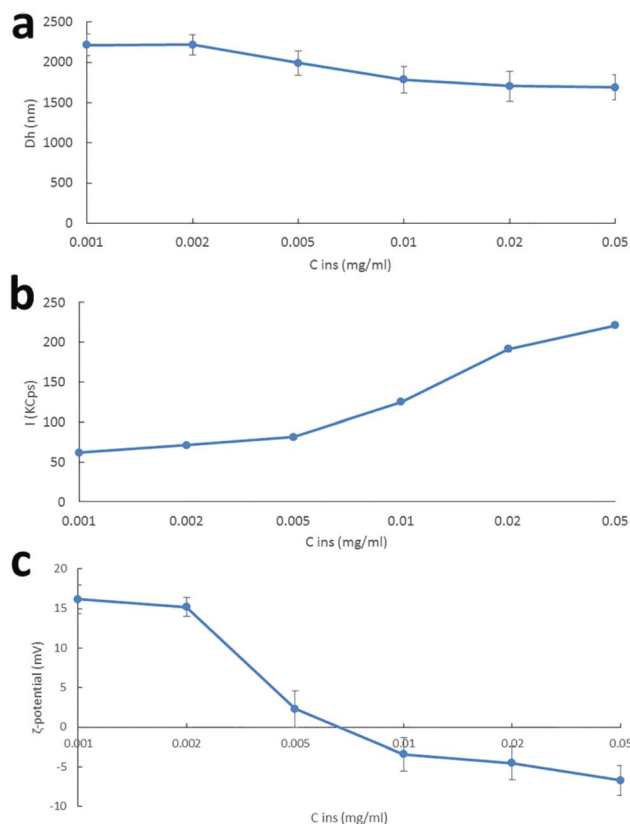
Nanoscale Advances

Paper

Fig. 5 (a) Hydrodynamic diameter and (b) scattering intensity over time, and (c) ζ-potential *versus* insulin concentration, of f-CNH:insulin complexes.

in Fig. 5. The increase in insulin concentration led to a decrease in the size and the size distribution, increase in the mass, and decrease in the zeta potential of the complexes (Fig. 5 and Table S3†). These alterations of the physicochemical characteristics of the complexes revealed the successful complexation between the **f-CNHs** and the model protein. It should be noted that when the concentration of insulin was 0.01 mg mL^{-1}, we observed a shift of the zeta potential from positive to negative values (Fig. 5 and Table S3†). As insulin concentration was increased,

each anino group of **f-CNHs** interacted successfully with an increasing number of insulin molecules, and the degree of charge neutralization became higher, as zeta potential values revealed. Additionally, the population of complexed particles became more homogenous, as the PDI values and size distribution curves show (Fig. S4†).

We also tested the loading capacity of the complexes. The results are presented in Table S3.† The loading efficiency is strongly dependent on the physicochemical characteristics of the complexes and partially dependent on the initial amount of added insulin at the formulation or complexation stage. The highest loading efficiency was observed when the initial concentration of insulin was 0.01 mg mL^{-1}. Generally, the loading efficiency was increasing with the increase in the initial amount of insulin. Then, it reached a plateau at 75% and remained unaffected, taking into account the SD values (Table S3†). The shift of the zeta potential to negative values means that there is insulin, which is free in the dispersion.

In vitro cellular toxicity

Despite the fact that CNHs were considered as a material with increased cellular toxicity, our results in EO771 cancer cells and in normal fibroblasts revealed that the **f-CNHs** showed minimal cellular toxicity with an IC$_{50}$ of 151 μg mL^{-1} and 349 μg mL^{-1}, respectively (Fig. 6). The minimal cellular toxicity renders this material a suitable nanocarrier for drug delivery systems. We should point out that pristine CNHs are not water soluble. For this reason, surface modification is very important for increasing water solubility, followed by the *in vitro* and *in vivo* evaluation using cellular lines and animal models, respectively. Additionally, the observed values for the toxicity of **f-CNHs** are comparable to those observed in the literature.[52]

Evaluation of the acute toxicity *in vivo*

The observed minimal *in vitro* cellular toxicity prompted us to further examine the toxicity of **f-CNHs** *in vivo*, and assess any potential acute toxicity. A high dose of 200 μL of **f-CNHs** at a concentration of 100 μg mL^{-1} was injected intraperitoneally to 6 C57/Bl6 mice, and 6 other mice (controls) received an equal amount of saline. The mice were monitored for any signs of
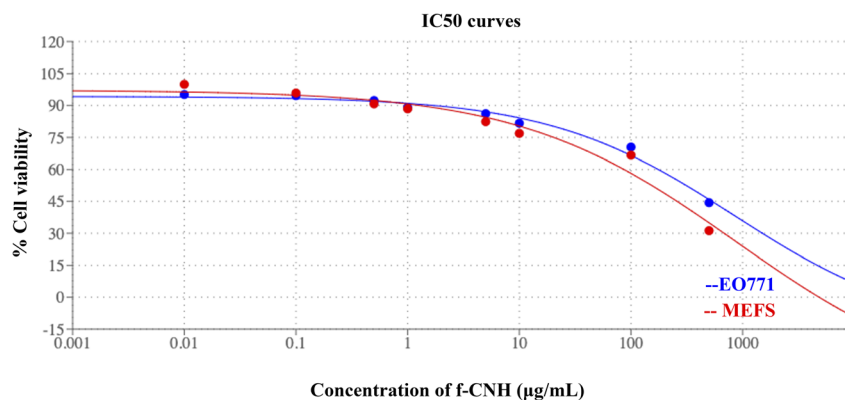

Fig. 6 IC$_{50}$ curves of cancer cell lines EO771 (blue) and normal fibroblasts MEFs (red) treated with various concentrations of **f-CNHs**.
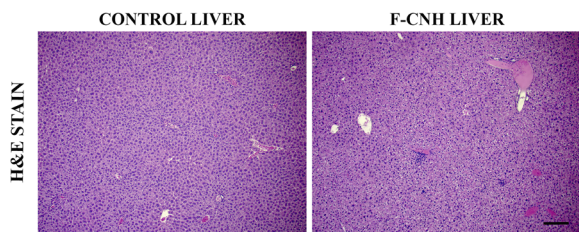
© 2023 The Author(s). Published by the Royal Society of Chemistry

Fig. 7 Hematoxylin and eosin staining of the livers of mice treated with saline and **f-CNHs**, respectively. The morphology of the hepatocytes and the infiltration of immune cells were similar in both the control and the treated groups. Representative images of the two groups are presented. The bar indicates 1000 μm.

discomfort for a period of 7 consecutive days. No visual signs of acute toxicity, signs of internal pain or discomfort, rough fur or impairment of movement was observed. The treated and the control mice were fed ad libitum, and no signs of reduction in appetite or loss of weight was observed in both groups. The mice remained well hydrated throughout the course of the experiment and no signs of de-hydration or loss of appetite in drinking water was observed. In general, a dose of 100 μg mL^{-1} of the **f-CNHs** was well tolerated with no signs of toxicity, which is in accordance with our *in vitro* results. The subsequent histological analysis of the mouse livers did not reveal any tissue necrosis, inflammation, or any visual signs of severe toxicity (Fig. 7).

Moreover, the histopathological analysis of the lungs and kidneys did not reveal any damage, or infiltration of immune cells, indicative of potential inflammation (Fig. S5†).

Conclusions

In conclusion, this work underscores the low toxicity observed in both *in vitro* and *in vivo* settings for CNHs modified with polyamidoamine dendrimers. Following the successful functionalization of CNHs with third-generation PAMAM dendrimers, we investigated their interactions with lipid bilayers to gain further insights. DSC measurements showed that the majority of interactions occurred between the modified CNHs and the polar groups of phospholipids, rather than being incorporated into the lipid chains themselves. In addition, the complexation of insulin was carried out using CNH-polyamidoamine dendrimers for the first time, while their stability assessment was realized through DLS and ELS techniques. The loading of insulin took place at different concentrations of this model protein, showing that the complexation is strongly dependent on the electrostatic interactions between the positive surface charge of **f-CNHs**, implying the added value of this functionalization for protein delivery. We proceeded to assess the potential harm caused by the modified CNHs by conducting tests on EO771 tumor cells and MEFs *in vitro*. The experiments showed that the CNH-polyamidoamine dendrimers are potential candidates due to their low cellular toxicity, as the IC50 values revealed. In order to further evaluate the safety of the modified CNHs, we conducted *in vivo* studies using mice. Upon performing histological analysis on the livers

of the mice, no indications of tissue necrosis, inflammation, or any visible signs of severe toxicity were observed. These findings strongly support the compatibility of the modified CNHs with living organisms and suggest their potential usefulness as platforms for delivery of substances with pharmaceutical and biomedical interest.

Conflicts of interest

There are no conflicts to declare.

References

1 Y. M. Lvov, P. Pattekari, X. Zhang and V. Torchilin, Converting poorly soluble materials into stable aqueous nanocolloids, *Langmuir*, 2011, **27**, 1212–1217.

2 Y. Zhu, P. Xu, X. Zhang and D. Wu, Emerging porous organic polymers for biomedical applications, *Chem. Soc. Rev.*, 2022, **51**, 1377–1414.

3 S. Sivagnanam, K. Das, M. Basak, T. Mahata, A. Stewart, B. Maity and P. Das, Self-assembled dipeptide based fluorescent nanoparticles as a platform for developing cellular imaging probes and targeted drug delivery chaperones, *Nanoscale Adv.*, 2022, **4**, 1694–1706.

4 S. Zhou, Q. Shang, N. Wang, Q. Li, A. Song and Y. Luan, Rational design of a minimalist nanoplatform to maximize immunotherapeutic efficacy: Four birds with one stone, *J. Controlled Release*, 2020, **328**, 617–630.

5 S. Zheng, Y. Tia, J. Ouyang, Y. Shen, X. Wang and J. Luan, Carbon nanomaterials for drug delivery and tissue engineering, *Front. Chem.*, 2022, **10**, 990362.

6 J. Ma, G. Wang, X. Ding, F. Wang, C. Zhu and Y. Rong, Carbon-based nanomaterials as drug delivery agents for colorectal cancer: clinical preface to colorectal cancer citing their markers and existing theranostic approaches, *ACS Omega*, 2023, **8**, 10656–10668.

7 C. Stangel and N. Tagmatarchis, Chemically functionalized carbon nanohorns for drug delivery applications, In *Functional materials in biomedical applications*, ed. C. Demetzos, N. Pippa and N. Naziris, Jenny Stanford Publishing Pte Ltd, 2023, 311–339.

8 A. Moreno-Lanceta, M. Medrano-Bosch and P. Melgar-Lesmes, Single-walled carbon nanohorns as promising nanotube derived delivery systems to treat cancer, *Pharmaceutics*, 2020, **12**, 850.

9 F. J. Rahmania, Y.-S. Huang, Y. A. Workie, T. Imae, A. Kondo, Y. Miki, R. Imai, T. Nagai, H. Nakagawa, N. Kawai and K. Tsutsumiuchi, Preparation of functional nanoparticles-loaded magnetic carbon nanohorn nanocomposites towards composite treatment, *Nanomaterials*, 2023, **13**, 839.

10 S. M. Hosseini, J. Mohammadnejad, R. Najafi-Taher, Z. B. Zadeh, M. Tanhaei and S. Ramakrishna, Multifunctional carbon-based nanoparticles: theranostic applications in cancer therapy and diagnosis, *ACS Appl. Bio Mater.*, 2023, **6**, 1323–1338.

11 S. K. Debnath and R. Srivastava, Drug delivery with carbon-based nanomaterials as versatile nanocarriers: Progress and prospects, *Front. Nanotechnol.*, 2021, **3**, 644564.

12 K. M. Isaac, I. V. Sabaraya, N. Ghousifam, D. Das, A. M. Pekkanen, D. K. Romanovicz, T. E. Long, N. B. Saleh and M. N. Rylander, Functionalization of single-walled carbon nanohorns for simultaneous fluorescence imaging and cisplatin delivery in vitro, *Carbon*, 2018, **138**, 309–318.

13 M. Zhang, M. Yang, C. Bussy, S. Iijima, K. Kostarelos and M. Yudasaka, Biodegradation of carbon nanohorns in macrophage cells, *Nanoscale*, 2015, **7**, 2834–2840.

14 K. Ajima, M. Yudasaka, A. Maigné, J. Miyawaki and S. Iijima, Effect of functional groups at hole edges on cisplatin release from inside single-wall carbon nanohorns, *J. Phys. Chem. B*, 2006, **110**, 5773–05778.

15 K. M. Isaac, I. V. Sabaraya, N. Ghousifam, D. Das, A. M. Pekkanen, D. K. Romanovicz, T. E. Long, N. B. Saleh and M. N. Rylander, Functionalization of single-walled carbon nanohorns for simultaneous fluorescence imaging and cisplatin delivery in vitro, *Carbon*, 2018, **138**, 309–318.

16 T. Murakami, J. Fan, M. Yudasaka, S. Iijima and K. Shiba, Solubilization of single-wall carbon nanohorns using a PEGdoxorubicin conjugate, *Mol. Pharm.*, 2006, **3**, 407–414.

17 S. Matsumura, K. Ajima, M. Yudasaka, S. Iijima and K. Shiba, Dispersion of cisplatin-loaded carbon nanohorns with a conjugate comprised of an artifcial peptide aptamer and polyethylene glycol, *Mol. Pharm.*, 2007, **4**, 723–729.

18 G. Pagona, N. Karousis and N. Tagmatarchis, Aryl diazonium functionalization of carbon nanohorns, *Carbon*, 2008, **46**, 604–610.

19 N. Pippa, C. Stangel, I. Kastanas, E. Triantafyllopoulou, N. Naziris, D. Stellas, M. Zhange, M. Yudasaka, C. Demetzos and N. Tagmatarchis, Carbon nanohorn/liposome systems: Preformulation, design and *in vitro* toxicity studies, *Mater. Sci. Eng.*, 2019, **105**, 110114.

20 J. Guerra, M. A. Herrero, B. Carrión, F. C. Pérez-Martínez, M. Lucío, N. Rubio, M. Meneghetti, M. Prato, V. Ceña and E. Vázquez, Carbon nanohorns functionalized with polyamidoamine dendrimers as efficient biocarrier materials for gene therapy, *Carbon*, 2012, **50**, 2832–2844.

21 J. Yang, Q. Zhang, H. Chang and Y. Cheng, Surface-engineered dendrimers in gene delivery, *Chem. Rev.*, 2015, **115**, 5274–5300.

22 N. Krathumkhet, T. Imae and M. P. Krafft, Nitric oxide gas in carbon nanohorn/fluorinated dendrimer/fluorinated poly(ethylene glycol)-based hierarchical nanocomposites as therapeutic nanocarriers, *ACS Appl. Bio Mater.*, 2021, **4**, 2591–2600.

23 B. He, Y. Shi, Y. Liang, A. Yang, Z. Fan, L. Yuan, X. Zou, X. Chang, H. Zhang, X. Wang, W. Dai, Y. Wang and Q. Zhang, Single-walled carbon-nanohorns improve biocompatibility over nanotubes by triggering less protein-initiated pyroptosis and apoptosis in macrophages, *Nat. Commun.*, 2018, **19**, 2393.

24 S. Zhu and G. Xu, Single-walled carbon nanohorns and their applications, *Nanoscale*, 2010, **2**, 2538–2549.

25 B. Li, X. Chen, W. Yang, J. He, K. He, Z. Xia, J. Zhang and G. Xiang, Single-walled carbon nanohorn aggregates promotes mitochondrial dysfunction-induced apoptosis in hepatoblastoma cells by targeting SIRT3, *Int. J. Oncol.*, 2018, **53**, 1129–1137.

26 C. Kuroda, K. Ueda, H. Haniu, H. Ishida, S. Okano, T. Takizawa, A. Sobajima, T. Kamanaka, K. Yoshida, M. Okamoto, T. Tsukahara, Y. Matsuda, K. Aoki, H. Kato and N. Saito, Different aggregation and shape characteristics of carbon materials affect biological responses in RAW264 cells, *Int. J. Nanomed.*, 2018, **5**, 6079–6088.

27 T. Nagai, N. Kawai, M. Gonda, K. Iida, T. Etani, D. Kobayashi, T. Naiki, A. Naiki-Ito, R. Ando, S. Yamaguchi, Y. Sugahara, S. Ueno, K. Tsutsumiuchi, T. Imae and T. Yasui, Role of HIKESHI on hyperthermia for castration-resistant prostate cancer and application of a novel magnetic nanoparticle with carbon nanohorn for magnetic hyperthermia, *Pharmaceutics*, 2023, **13**, 626.

28 E. C. Ekwueme, R. Rao, M. Mohiuddin, M. Pellegrini, Y. S. Lee, M. P. Reiter, J. Jackson and J. W. Freeman, Single-walled carbon nanohorns modulate tenocyte cellular response and tendon biomechanics, *J. Biomed. Mater. Res., Part B*, 2020, **108**, 1907–1914.

29 K. Kokubun, S. Matsumura, M. Yudasaka, S. Iijimam and K. Shiba, Immobilization of a carbon nanomaterial-based localized drug-release system using a bispecific material-binding peptide, *Int. J. Nanomed.*, 2018, **16**, 1643–1652.

30 K. J. Shah and T. Imae, Selective gas capture ability of gasadsorbent-incorporated cellulose nanofiber films, *Biomacromolecule*, 2016, **17**, 1653–1661.

31 Y. Lu, D. L. Slomberg, A. Shah and H. Schoenfisch, Nitric oxide-releasing amphiphilic poly (amidoamine)(PAMAM) dendrimers as antibacterial agents, *Biomacromolecules*, 2013, **14**, 3589–3598.'.

32 M. Fana, J. Gallien, B. Srinageshwar, G. L. Dunbar and J. Rossignol, PAMAM dendrimer nanomolecules utilized as drug delivery systems for potential treatment of glioblastoma: a systematic review, *Int. J. Nanomed.*, 2020, **15**, 2789–2808.

33 H. Kheraldine, O. Rachid, A. M. Habib, A.-E. A. Moustafa, I. F. Benter and S. Akhtar, Emerging innate biological properties of nano-drug delivery systems: A focus on PAMAM dendrimers and their clinical potential, *Adv. Drug Delivery Rev.*, 2020, **178**, 113908.

34 L. J. Fox, R. M. Richardson and W. H. Briscoe, PAMAM dendrimer - cell membrane interactions, *Adv. Colloid Interface Sci.*, 2018, **257**, 1–18.

35 M. Ciolkowski, J. F. Petersen, M. Ficker, A. Janaszewska, J. B. Christensen, B. Klajnert and M. Bryszewska, Surface modification of PAMAM dendrimer improves its biocompatibility, *Nanomed.: Nanotechnol. Biol. Med.*, 2012, **8**, 815–817.

36 Y. Fan, F. Su, K. Li, C. Ke and Y. Yan, Carbon nanotube filled with magnetic iron oxide and modified with polyamidoamine dendrimers for immobilizing lipase

toward application in biodiesel production, *Nat. Sci. Rep.*, 2017, **7**, 45643.

37 P. Melgar-Lesmes, A. Luquero, M. Parra-Robert, A. Mora, J. Ribera, E. R. Edelman and W. Jiménez, Graphene-dendrimer nanostars for targeted macrophage overexpression of metalloproteinase 9 and hepatic fibrosis precision therapy, *Nano Lett.*, 2018, **18**, 5839–5845.

38 K. H. Wong, Z. Guo, M.-K. Law and M. Chen, Functionalized PAMAM constructed nanosystems for biomacromolecule delivery, *Biomater. Sci.*, 2023, **11**, 1589–1606.

39 N. Pippa, D. D. Chronopoulos, D. Stellas, R. Fernández-Pacheco, R. Arenal, C. Demetzos and N. Tagmatarchis, Design and development of multi-walled carbon nanotube-liposome drug delivery platforms, *Int. J. Pharm.*, 2017, **528**, 429–439.

40 M. Luo, H. Wang, Z. Wang, H. Cai, Z. Lu, Y. Li, M. Du, G. Huang, C. Wang, X. Chen, M. R. Porembka, J. Lea, A. E. Frankel, Y.-X. Fu, Z. J. Chen and J. Gao, A STING-activating nanovaccine for cancer immunotherapy, *Nat. Nanotechnol.*, 2017, **12**, 648–654.

41 L. Zhiyu, T. P. Allan and T. A. Gill, Encapsulation of bioactive salmon protein hydrolysates with chitosan-coated liposomes, *J. Funct. Foods*, 2015, **19**, 733–743.

42 H. Nakajima, K. Kobashi, C. Stangel, T. Morimoto, M. Zhang, N. Tagmatarchis and T. Okazaki, Step-by-step characterization of a series of polyamidoamine dendrons on carbon nanohorn surface, *Appl. Surf. Sci.*, 2023, **624**, 157077.

43 C. Demetzos, Differential scanning calorimetry (DSC): a tool to study the thermal behavior of lipid bilayers and liposomal stability, *J. Liposome Res.*, 2008, **18**, 159–173.

44 R. Koynova and M. Caffrey, Phases and phase transitions of the phosphatidylcholines, *Biochim. Biophys. Acta*, 1998, **1376**, 91–145.

45 J. D. Nickels, J. C. Smith and X. Cheng, Lateral organization, bilayer asymmetry, and inter-leaflet coupling of biological membranes, *Chem. Phys. Lipids*, 2015, **192**, 87–99.

46 S. Hong, P. R. Leroueil, E. K. Janus, J. L. Peters, M. M. Kober, M. T. Islam, B. K. Orr, J. R. Baker and M. M. Banaszak Holl, Interaction of polycationic polymers with supported lipid bilayers and cells: nanoscale hole formation and enhanced membrane permeability, *Bioconjugate Chem.*, 2006, **17**, 728–734.

47 Y. Wang, Y. Zheng, L. Zhang, Q. Wang and D. Zhang, Stability of nanosuspensions in drug delivery, *J. Controlled Release*, 2013, **172**, 1126–1141.

48 B. Derjaguin and L. Landau, Theory of the stability of strongly charged lyophobic sols and of the adhesion of strongly charged particles in solutions of electrolytes, *Acta Physicochim. URSS*, 1941, **14**, 633.

49 E. J. W. Verwey and J. Th. G. Overbeek, Theory of the stability of lyophobic colloids, *J. Phys. Colloid Chem.*, 1948, **51**, 631–636.

50 N. Feliu, P. Kohonen, J. Ji, Y. Zhang, H. L. Karlsson, L. Palmberg, A. Nyström and B. Fadeel, Next-generation sequencing reveals low-dose effects of cationic dendrimers in primary human bronchial epithelial cells, *ACS Nano*, 2015, **9**, 146–163.

51 C. Jeworrek, O. Hollmann, R. Steitz, R. Winter and C. Czeslik, Interaction of IAPP and insulin with model interfaces studied using neutron reflectometry, *Biophys. J.*, 2009, **96**, 1115–1123.551.

52 J. Miyawaki, M. Yudasaka, T. Azami, Y. Kubo and S. Iijima, Toxicity of single-walled carbon nanohorns, *ACS Nano*, 2008, **2**, 213–226.